SPE-199753-MS

Pulsed Power Plasma to Enhance Near Wellbore Permeability and Improve Well Performance

Ali Rezaei and Fahd Siddiqui, University of Houston; Nicole Callen and Peter Gordon, ExxonMobil Research & Engineering; Waylon House; Mohamed Soliman, University of Houston

This paper was prepared for presentation at the SPE Hydraulic Fracturing Technology Conference and Exhibition held in The Woodlands, Texas, USA, 4-6 February 2020.

Abstract

Unconventional reservoirs suffer from an ultra-low permeability, causing their drainage area to be limited to tens of feet. An efficient technique that can be used in combination with conventional hydraulic fracturing to increase the drainage area is pulse power plasma. In this study, we used an experimental approach to study the effect of pulsed power plasma discharge on the permeability change around wellbore under tri-axial confining stress conditions.

We designed and used equipment, allowing for the generation of the shock wave in a true tri-axial cell to perform the analysis in this study. The equipment has a capacity for rock samples of 14 *in* on each edge with 1.5 *in* diameter well in the center. Using the equipment, the stored electrical energy in capacitors is instantaneously released into a fusible link creating a thermite reaction, which creates a shock wave in the wellbore and is transmitted to the rock afterward. The shock wave affects the permeability of samples, even in situations where the generated stress loading is below rock strength.

Several types of material, such as limestone, sandstone, and concrete are tested in this study. Samples were investigated before and after the electrohydraulic discharge to find the extent and magnitude of the induced fractures (permeability enhancement) and their relationship with the released energy. Also, the effect of repetitive low-magnitude shock waves for creating micro-cracks in rock is studied. It is observed that even under sub-critical loading conditions, micro-cracks are generated in the rock samples that might be a result of the main shockwave or reflection of the stress wave from the boundary. These fractures were less controlled by the stress orientation as compared with hydraulic fractures. However, they contributed to the permeability enhancement around the wellbore that can be up to orders in magnitude. Finally, the optimum discharge energy for the maximum permeability enhancement is suggested.

In this study, for the first time, we tested the rock under confining stresses and imaged them using computer tomography (CT) scanning. Also, change of permeability around the wellbore using pulse power plasma is a novel use of pulse fracturing technology that can effectively be mixed with hydraulic fracturing treatment in unconventional reservoirs and maximize the stimulated reservoir volume (SRV). The results of this paper can help to maximize the EUR from the reservoir.

Introduction

Electrohydraulic (also known as pulse power plasma) discharge is a reliable waterless method that can be used to stimulate near wellbore region. Unlike conventional hydraulic fracturing that requires a considerable amount of water, this technique only requires the wellbore to be filled with water. Also, in this technique, the fracture propagation is less affected by stress shadowing due to the propagation of multiple fractures from the same or opposite directions (Rafiee et al., 2015; Rezaei et al., 2015). In this study, we aim at enhancing the permeability of near-wellbore regions of different rock samples using electrohydraulic discharge underwater. Macroscopic fractures can enhance the permeability by orders of magnitudes. To avoid creating major fractures and destroying the samples, we used low power electrohydraulic discharges to induce only microscopic fractures (to enhance permeability). This approach can be used to stimulate the near-wellbore region of the unconventional reservoir were the drainage area would be limited to a few feet from hydraulic fractures and wellbore, otherwise.

The first usage of electricity as the oil well stimulation technique was reported in 1964 on oil shale (Melton and Cross, 1968). Since then, other techniques such as explosive and electrohydraulic discharge have been used in combination with hydraulic fracturing or as a standalone technique for stimulation of the low permeability reservoir rocks. Electrohydraulic fracturing of rock is composed of two main processes, namely electrical and mechanical. The electrical process involves storing and discharging the electrical energy from capacitors to electrodes that are located in the wellbore. As a result of the discharge, a high energy plasma forms between the electrodes. The plasma generates a high-pressure shock wave in the rock and can induce damage in the rock, depending on the magnitude of the output energy from capacitors.

There are two types of discharges using this technology, namely pulsed corona electrohydraulic discharge (PCED) and pulsed arc electrohydraulic discharge (PAEC) (Touya et al., 2006). In PCED, a streamer of the corona is formed in water. The whole process of PCED takes up to 100 n sec and generates weak shock waves. On the contrary, in the second type, the duration of the applied voltage is in the microseconds order, and it generates higher energy. In PAEC, a high energy plasma, that depends on the magnitude of the applied voltage and the distance between electrodes, is formed between the electrodes. Also, a metal fusible link (ionizable) and an aqueous environment between electrodes can be used to enhance the generated pressure as the result of the reaction of the wire with aqueous material. In this study, we investigate the PAEC process in our experiments and use aluminum as the fusible link.

Three main categories have attracted the research attentions on electrohydraulic shockwave in the last decade. These categories are electrical, mechanical, and electromagnetic processes (La Borderie et al., 2016). The electrical part includes storing the electrical energy, discharging the energy, the relationship of discharged energy with the generated pressure (Touya et al., 2006; Li et al., 2016), surrounding environment of electrodes, and the properties of the electrodes. Examples include the effect of water gap (Zhu et al., 2014), electrical wire and other environments such as glycerol (Rososhek et al., 2017), design of the electrodes, stored and released energy (Kuznetsova et al., 2014; Kuznetsova et al., 2015; Koutoula et al., 2016; Ageev et al., 2019), explosions of different metal wires in water (Han et al. 2018; Rososhek et al., 2018), etc. In the mechanical part of the electrohydraulic shock wave generation, which has been studied mainly using experimental and numerical approaches, the focus of the literature has been on the induced damage (micro and macro fractures) in the rock from the geomechanics perspective. In this category, problem such as the mechanism of rock failure using pulse fracturing and dynamic loading (Safari et al, 2015), number and quality of the generated fractures (Xiao et al., 2018; Bian et al., 2018), effect of multiple discharges on the generated fractures and proppant placement (Riu et al., 2019), etc. are studied. The electromagnetic field generated by the electrical discharge is the third category that has been the subject of a few studies. This category has a potential application in fracturing treatment and SRV estimation, and it was studied numerically by Xiao et al. (2018).

Electrohydraulic discharge has been used as a method for enhancing the near-wellbore permeability of the rock (Reess et al., 2009; Maurel et al., 2010; Chen et al., 2013). It is observed that the permeability of rock in the proximity of the discharge can be enhanced without creating macroscopic fractures. Maurel et al. (2010) described an experimental setup for quantifying the effect of plasma discharge on the permeability enhancement of mortar samples. Their study showed that the permeability enhancement shows a positive correlation with applied energy and the number of plasma discharges. The authors noted the existence of a threshold for maximum amplitude of the shockwave above which damage is observed. They reported a permeability increase by two orders of magnitude for the repetitive shots. Chen et al. (2013) presented an anisotropic damage model for the evolution of rock permeability. They conducted experiments for determining the effect of discharge load under low and high confining stresses on the rock permeability. Although several studies have shown the effect of electrohydraulic discharge on the permeability change, there is still a lack of understanding about these effects under reservoir conditions with confining stresses.

In this study, we used an experimental approach to study the effect of the electrohydraulic discharge on the permeability enhancement around wellbore under tri-axial confining stress conditions. We tested a total of 11 samples, among which five were cement, three limestones, and three sandstones. Three cement samples were used in single discharge experiments, and two samples were used to investigate the effect of repetitive shocks. The cement samples for single discharge experiments were tested without confining stresses and with perforated PVC pipes to represent the cased wellbore. The other samples, including the cement blocks for repetitive discharges, were tested under confining stresses. In the next section, the experimental setup and the mechanism of pulse power plasma generation are reviewed. Then, a detailed analysis of the experiment results is presented in the discussion and result section. Finally, the conclusions are drawn. We demonstrate several advantages of this technique over conventional hydraulic fracturing. For example, this technique is much cheaper than conventional hydraulic fracturing, can be combined with the regular hydraulic fracturing, and uses a very small amount of water and chemicals.

Experimental Set-Up

A pulse plasma generation equipment was designed with the output capacity of up to 20 kJ of electrical energy. The equipment consists of three major components: an electrical component, a true tri-axial cell, and a monitoring and recording system. The following sections describe different pieces of the equipment, the geometry of the rock samples, the experiment results, and discussion.

Electrical Component

The electrical unit (Figure 1a) is responsible for storing and releasing electrical energy. It houses the high voltage charging system, capacitors, and the spark-gap switch. The electrical energy is stored in two 40 kV capacitors of 12.5 μF capacitance (Figure 1b). The charging energy is provided by a high capacity/high ramping rate high voltage supply. A spark-gap switch provides a mechanism of triggering the discharge. The air pressure controls the threshold voltage in the spark-gap switch, and discharge occurs through a secondary Marx generator to initiate arc formation. The stored electrical energy in the capacitors is transferred to the wellbore using three high-voltage cables (Figure 1c) from the top of the triaxial cell. The cables are connected to two parallel and insulated copper rods (Figure 1d) through which the depth at which pulse discharge occurs is controlled. At the end of the two rods, a metal wire (Aluminum in this study) is attached to serve as a fusible link. The high voltage causes the link to vaporize and give rise to plasma generation and shockwave expansion. The sudden expansion provides the mechanical energy for generating multiple fractures in the test sample.

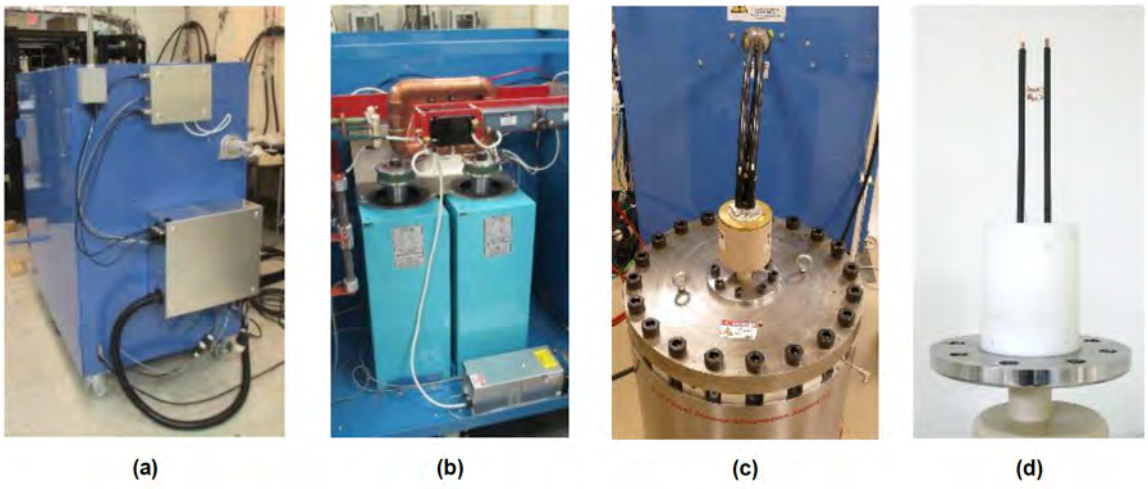

Figure 1—Electrical component: (a) container cabinet (b) capacitors and spark gap (c) High voltage cables are connected to the cell from top (d) electrodes and fusible link.

Triaxial Cell

The triaxial cell houses the sample and provides the mechanism for applying the three principal stresses on the sample. Figure 2a shows the inside of the cell and metal plates that apply the confining stresses. The cell has three fixed plates (two on the sides and one on the top), and two of them are shown in Figure 2a. The stresses are applied by hydraulic actuators (Figure 2b). The triaxial cell has an opening from the top for lowering the electrodes. The sample is lowered and placed inside the cell, and other plates are placed around it (Figure 2c). The maximum sample dimensions that can be fit in the cell are 14″×14″×14″.

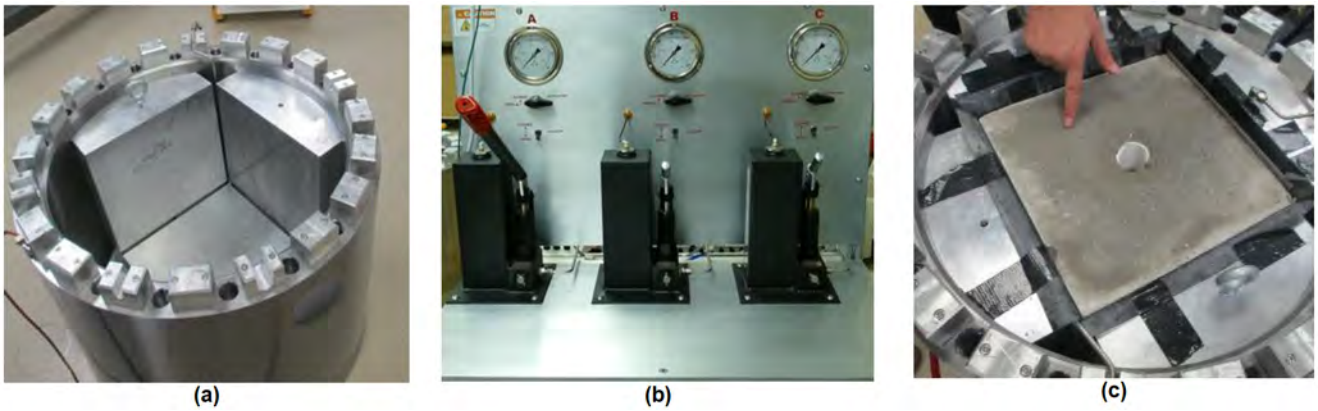

Figure 2—Triaxial cell (a) Tri-axial cell with hydraulic pumps (b) two fixed plates on the sides and the vertical actuator on the bottom (c) sample and all horizontal plates on the sides.

Monitoring and Recording System

The monitoring and recording system (Figure 3) consists of fast pressure gauges, electronic oscilloscopes, remote triggering mechanisms, and a computer for gathering data from the scopes. The pressure gauges are connected to the oscilloscopes, and from there, everything is connected to a PC for recording the voltage, electric current, and pressures. Figure 2a shows the software used for recording the experiment parameters.

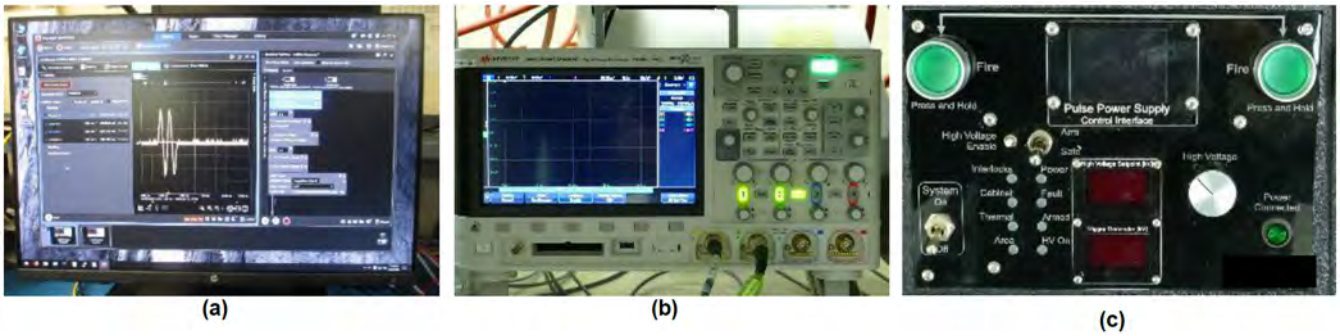

Figure 3—Monitoring and recording system (a) Keysight Benchvue software (b) oscilloscope (c) remote triggering.

Discussion and Results

The changes of permeability using a pulse generated shockwave has been previously investigated on smaller samples and with no confining stresses (Maurel et al., 2010). Permeability changes in the rock sample can be plotted as a function of induced fractures (or damage), the stress generated by the shockwave, strain of the rock, and the pressure wave that does not necessarily generate uniform stress on the wellbore surface. Figure 4a shows the result of permeability change as a function of the pressure on the rock sample. The pressure is calculated from the output energy of the capacitors (Touya et al., 2006). As can be seen in the figure, there is a threshold pressure, after which the permeability of the rock increases. In the example in Figure 4a, that was performed on the mortar sample, it can be observed that the permeability starts to increase for pressures higher than 90 MPa, which is about four times the material strength, and that is because the load was dynamic. Also, the figure shows that the permeability changed by two orders of magnitude for a pressure of 250 MPa. Moreover, the change of permeability showed a linear relationship with the number of discharges (Figure 4b). It can also be seen in the figure that as the number of discharges increases, the permeability of the sample increases.

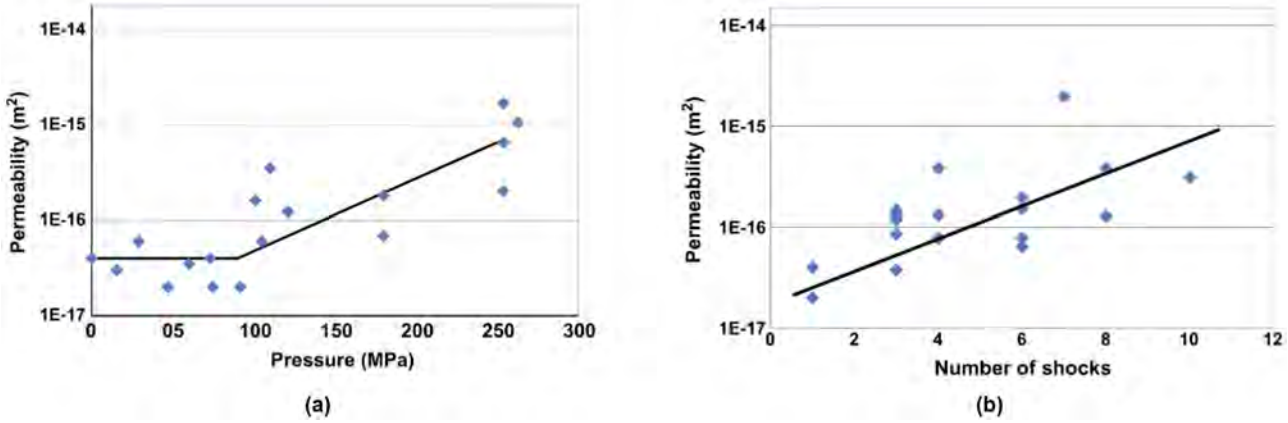

Figure 4—Change of permeability as a function (a) applied pressure generated by electrohydraulic discharge (b) number of shocks (after Maurel et al. (2010))

Based on the observations for energy output (which was converted to pressure on the rock surface in the previous example) and the number of discharges in enhancing permeability, in this study, two types of experiments were conducted on different rock samples. The first set of experiments consisted of single discharges on cement, sandstone and limestone blocks. Three blocks from each material were subjected to increasing discharge energy. The second set of experiments consisted of multiple shots on two confined cement samples. Four pulses were discharged into cement samples in the repetitive discharge experiments, and a qualitative measurement on the number of induced micro and macro fractures was taken between the

shots. It should be noted that there was no confining stress applied to the cement blocks that were used for the single discharge experiments. The confining stresses for the other six samples and the two samples under repetitive discharges were 250, 200, and 300 psi for σ_H, σ_h, and σ_v respectively.

A comparison between the electrical explosions of different metal wires in water presented by Han et al. (2018). They concluded that copper wires always generated the strongest shock waves. Also, they observed that the wire explosions for Aluminum, Titanium, and Iron were accompanied by chemical reactions between water and the metal wire. Therefore, in all the experiments, we used the Aluminum wire of 22 AWG (0.0253 in). All eleven blocks were collected, cut into squares or slabs and analyzed using a computer tomography (CT) scan after the experiments. Sandstone blocks were cut into eight 7×7×7 inch cubes because of the size limitation in CT scan and handling (Figure 5a), while cement and limestone cubes were cut into 2″ slabs of 2×7×14 sizes (Figure 5b). Figure 5a and b show the cut for sandstone blocks and other rock types, respectively.

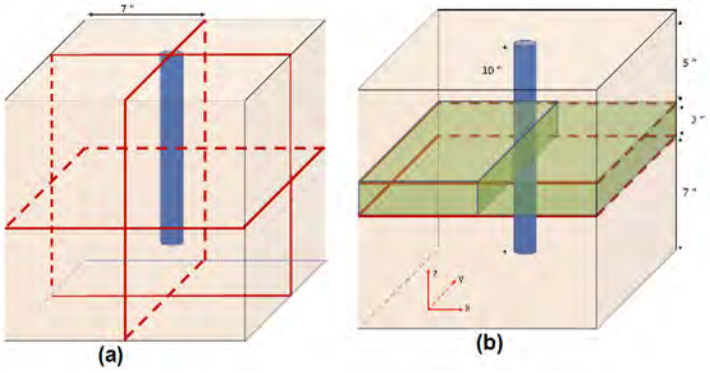

Figure 5—Sample cutting schematics. a) 7×7×7 inch cubes for sandstone b) 2×7×14 inch slabs for other material.

Extent and Magnitude of the Induced Micro and Macro Cracks

It is observed that, even under loading conditions that do not initiate macro fractures, micro-cracks are generated in the rock samples. Also, the stress shock wave may cause a rearrangement in the rock grains and improvement of permeability. Our goal in this study is to quantify the magnitude and extension of the induced micro and macro cracks that can help to enhance permeability. Such quantification can be done by CT scanning and other conventional permeability measurement techniques (such as double packer test) on smaller rock samples, as discussed in previous studies (Maurel et al., 2010; Riu et al., 2019). We observed that the generated fractures were less influenced by applied stress orientations than expected in hydraulic fractures. This might be due to the relatively low stress anisotropy that we used in this study. For more discussions on underground stresses and their impact on the hydraulic fracturing process, one may refer to Soliman and Dusterhoft (2016). As discussed in the previous section, despite their small size, the microscopic fractures can contribute to the permeability enhancement around the wellbore by up to two orders of magnitude. Hence, we tried to avoid creating macro fractures in the rock, although some fractures were generated, and try to determine the highest energy that leads to microscopic cracks only.

Cement samples

Based on our previous experiments on unsaturated cement blocks, we estimated that eight kJ would destroy the cement blocks completely. Therefore, three tests with 2.2 kJ, 4.3 kJ, and 6.4 kJ discharge energies were conducted on the samples. We started by 2.2 kJ as our first test and wanted to examine whether this energy level will create any fractures in the rock. We observed no fractures at this level of energy. Next, we investigated the 4.3 kJ, and a narrow crack was induced that extended from the wellbore toward the outer boundary. Since major fractures were not observed in this case, we increased the energy to 6 kJ as our last

energy input. However, six kJ discharge energy created three major cracks that extended to the boundary of the sample, thereby breaking the sample in three major chunks (Figure 6e). It should be mentioned again that no confining stress was applied in these three tests and samples recovered after each discharge. A summary of the tests on cement blocks are given in Table 1.

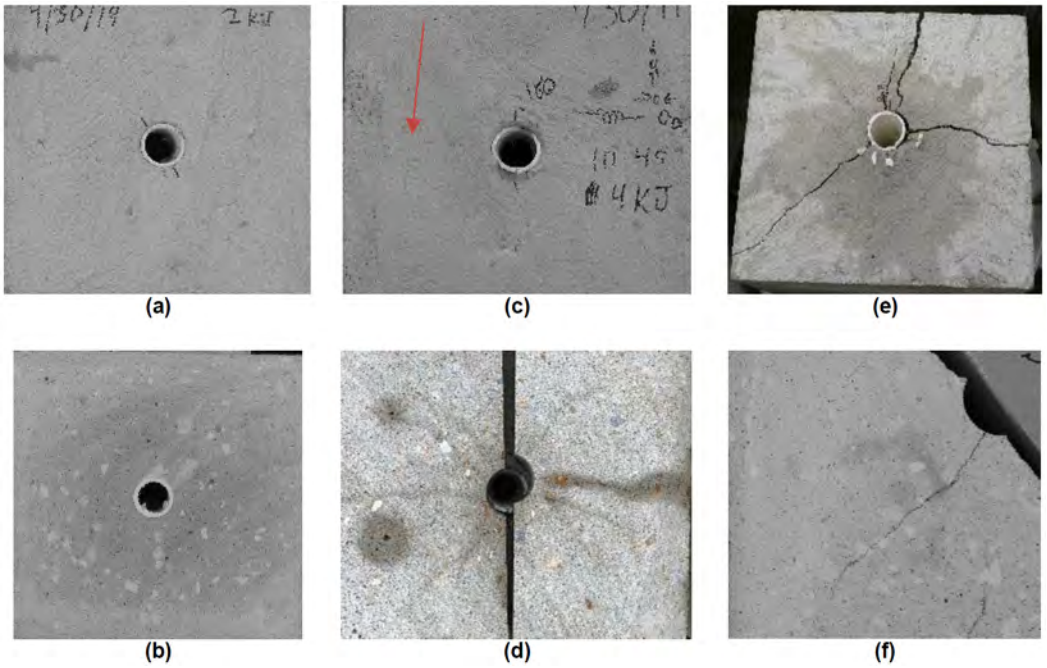

Figure 6—Induced fractures into the cement samples for (a,b) 2.2 kJ, (c,d) 4.3 kJ, (e,f) 6.4 kJ discharges.

Table 1—Summary of single-shot permeability enhancement study on cement samples.

Sample #	Energy	Observations
1	2.2	No visible fractures
2	4.3	Some small cracks
3	6.4	Sample broke in three pieces

Figure 6 shows the tested cement samples after the electrohydraulic discharge. As said before, our first step was to investigate the samples for any observable cracks. Figure 6a-b show the results for the 2 kJ test, and as can be seen, no visible fractures was observed on the surface (Figure 6a) or slabbed section (Figure 6b) for this case. In the second test, as shown by the red arrow in Figure 6c, a narrow crack was observed from wellbore that extended to the outer boundary of the sample. More interestingly, we observed multiple of these cracks in the slabbed piece, at the depth where the electrodes were located (~ 6 inches from sample top). These cracks are shown in Figure 6d and became visible after we pour some water on the sample and let it dry. For the case of 6.4 kJ discharge energy, three fractures were observed that extended to the boundaries of the sample both in horizontal and vertical directions (Figure 6e-f). In terms of the goals that we had for this paper, this test was not successful as it created relatively large fractures in the sample. However, we slabbed the sample to see if the CT scanning will reveal the extent of microscopic cracks (increase in permeability).

Limestone samples

For the limestones, we selected a higher starting energy compared with cement. The same procedure, as for the cement samples, was taken for this set of experiments. The energy that we selected for the limestone samples were 6.4 kJ, 8.7 kJ, and 11.9 kJ. We started by the least energy, and no visible fracture was observed. The discharge energy was then increased to 8.7 kJ, and we still did not see any visible cracks in the sample. Finally, we increased the discharge energy to 11.9 kJ. At this level, we observed multiple cracks around the wellbore and in the slab. A summary of the observations is presented in Table 2.

Table 2—Summary of single-shot permeability enhancement study on limestone.

Sample #	Energy	Observations
1	6.4	Minor surface cracks
2	8.7	No visible cracks
3	11.9	Multiple cracks observed around the wellbore

Figure 7 shows the visual investigation of the limestone samples for the largest discharge energy. Red arrows around the wellbore mark the fractures that were induced in the sample in Figure 7a. We also observed a crack that did not seem to have been initiated from the wellbore and is marked with a blue arrow in the figure. Also, in the area in front of the fusible links where we cut the slab (Figure 7b), a fracture was observed that extended from wellbore to the outer face of the sample. The fracture is marked with a green arrow in Figure 7b.

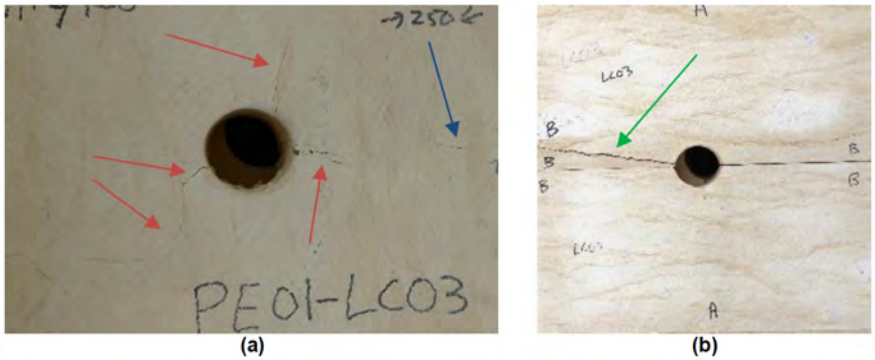

Figure 7—Induced fractures in the limestone samples for 11.9 kJ discharge (a) surface of the sample (b) middle of the sample in front of the fusible links.

Sandstone samples

We started the first sandstone test with 4.1 kJ, and no fractures were observed for this energy level. Hence, the next test was run by 5.5 kJ discharge, and we applied our last discharge at 8.7 kJ. Although we did not see any visible cracks for the first two cases, in the case of 8.7 kJ discharge energy, we observed two horizontal cracks along with the layer bedding. The results of the visual investigation for the sandstone samples are summarized in Table 3.

Table 3—Summary of single-shot permeability enhancement study on Sandstone samples.

Sample #	Energy	Observations
1	4.1	No visible cracks
2	5.5	No visible cracks
3	8.7	Two horizontal fractures observed

Figure 8a-d show the sandstone samples after the discharges. As can be seen, no visible crack was observed for discharge energies of 4.4 kJ and 5.5 kJ (Figure 8a and b). For the case of 8.7 kJ discharge energy, although no visible crack was observed around the wellbore, two horizontal cracks were observed along the layer lines that are marked with red arrows in Figure 8d. It should be noted that the wellbore was drilled perpendicular to the sample's bedding layer in all of the sandstone cases.

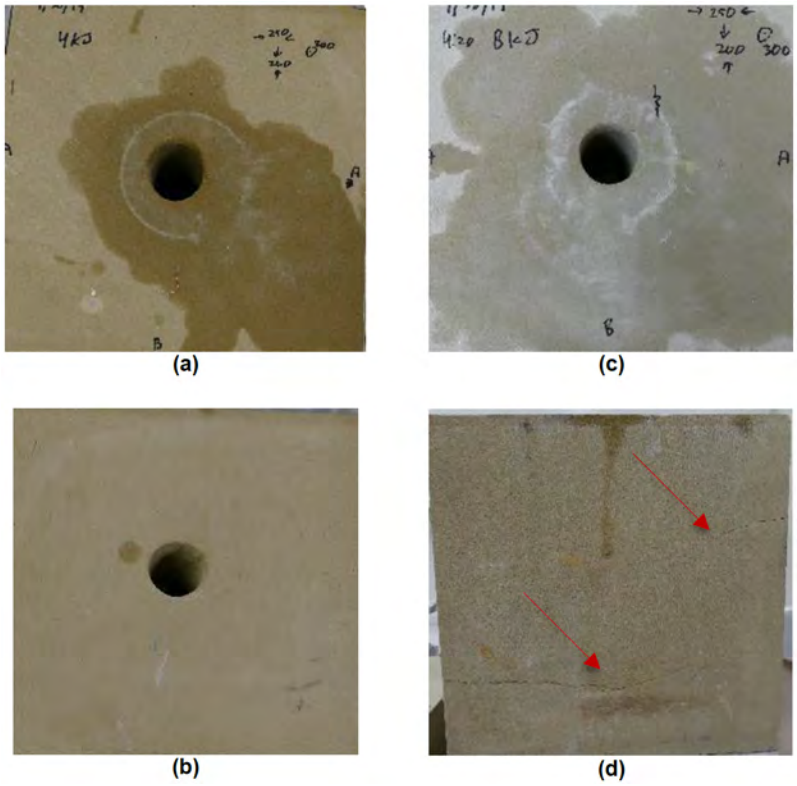

Figure 8—Induced fractures in the sandstone samples for (a) 4.1 kJ, (b) 5.5 kJ, (c,d) 8.7 kJ discharges.

Computed tomography scanning of the sandstone samples. As said earlier, the sandstone samples were cut to 8 pieces as shown in Figure 5a. After the discharges, CT scans were used to investigate the induced fractures inside the rock samples. The CT data were captured in a Nikon XT H225 ST scanner with a 225 kV rotating target. The specimen was exposed to broad-spectrum radiation with a copper filter to remove lower energy parts of the photon flux. Data were collected at 225 keV, impinging on a target with a focal spot size of 50 mm. Imaging was conducted with 7500 projections as the sample was rotated through (*360°*). Total acquisition time on a 7 inch cubic samples was approximately 10 hours. 3-D images were generated with Nikon's CT reconstruction software with a voxel resolution of 100 mm, including beam hardening corrections and noise reduction. In the rest of this section, we present the result of two CT scans of the induced fractures inside one 7-inch cube piece of the sandstone sample that was exposed to 8.7 kJ discharge. In each of these examples, three planes (we refer to them as red, blue, and green planes) are selected orthogonal to each other, and the induced fractures are shown and discussed on these planes separately.

Figure 9 shows the first configuration of the three planes and induced cracks in the sandstone sample on those planes. In this case, the red plane is the x-y plane (z-axis is aligned along the wellbore direction in all of the examples) just below where the wellbore ends, blue is the x-z plane that intersects the wellbore, and green is the y-z plane close to the outer boundary of the sample (Figure 9a). Figure 9b shows the induced cracks on the red plane. The wellbore can be seen on the bottom right of the figure. Also, there is a small fracture on the bottom left of the sample that is believed to be due to the shockwave reflection from the

boundary. Figure 9c shows the induced fractures on the blue plane. Two fractures were observed on this plane that are shown by white arrows. The first fracture started from a corner of the deepest point at the wellbore and continued toward the bottom of the sample with a *45°* angle. The presence of this fracture is interesting as it stopped in the middle of block and is believed to be purely due to electrohydraulic discharge. The second fracture initiated from one of the outer boundaries of the sample and propagated parallel to the first fracture. We observed this fracture after the test and believe that it is a result of the stress wave reflection from the boundary. Also, some fractures were observed on the green plane (Figure 9d). These cracks are the cross section of the same fracture shown with white arrows in Figure 9a, and the bottom left fracture shown in Figure 9c on the green plane.

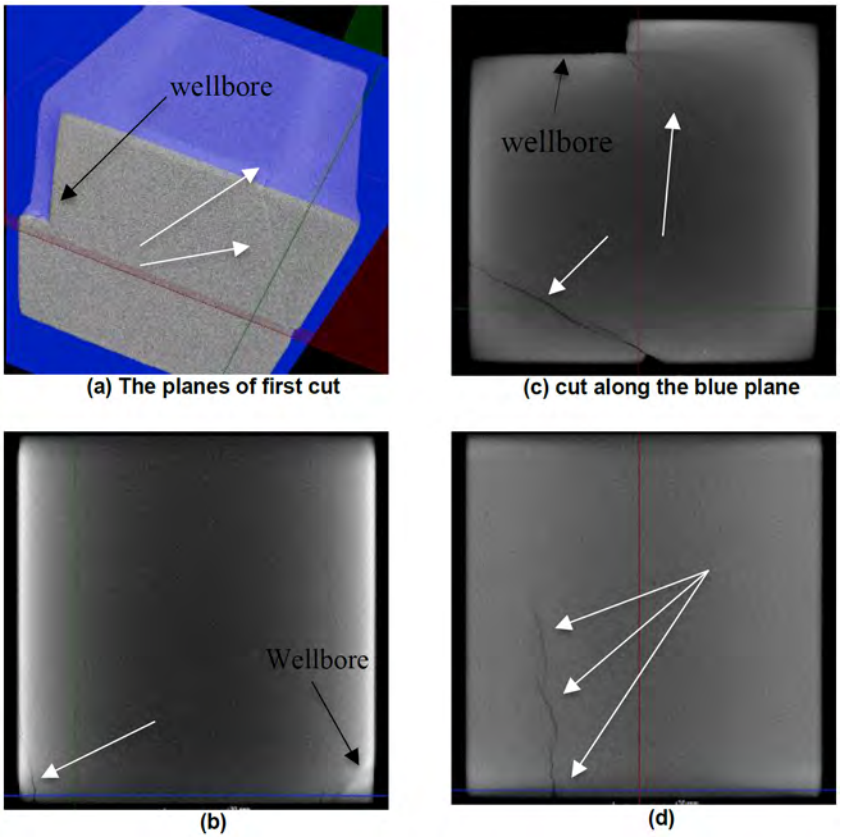

Figure 9—The first example of the induced fractures in the sandstone sample. (a) orthogonal planes (red, blue, and green), (b-d) induced fractures on the red, blue, and green planes, respectively.

In the second example, the green plane is the x-y (horizontal) plane cutting through the sample at some point in the wellbore, the red plane is the y-z plane in the middle of the sample, and the blue plane is the x-z plane with a larger distance from the sample boundary compared with the green plane in the previous example. Figure 10a shows the configuration of the planes for this example. Figure 10b shows the induced fractures on the red plane and as can be seen, the same fracture (with *45°*) which was observed in the last example, extended from one edge of the block to the other. Similarly, another fracture started from one side of the block and extended to the middle of the block. This fracture is shown with white arrows in Figure 10c. Also, as can be seen in the figure, this fracture did not extend all the way to the opposite edge and stopped in the middle of sample on the green plane. The same fracture can be seen on the blue plane as shown in Figure 10d.

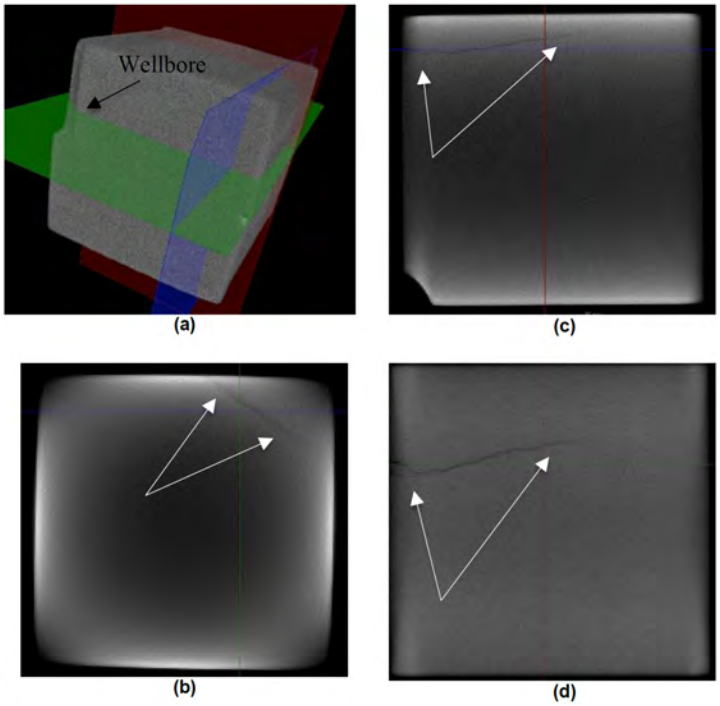

Figure 10—The second example of the induced fractures in the sandstone sample. (a) arbitrary orthogonal planes (red, blue, and green), (b-d) induced fractures on the red, green, and blue planes, respectively.

Repetitive Pulses and Stress Orientation

Two experiments were conducted on two similar concrete blocks to investigate the effect of repetitive charges and perforation direction with respect to the orientation of stresses. Four multiple pulses of 10 kJ were discharged on each sample. Both blocks had perforations at 180-degree phasing. The test conditions for both blocks were the same except that the maximum stress orientations were parallel (Figure 11) and perpendicular (Figure 12) to the perforations in the samples. We recovered and did the same visual observations after each discharge for this case. After the fourth discharge, we cut the core samples and performed X-Ray tomography for further analysis. The details of the two tests are discussed in the following section.

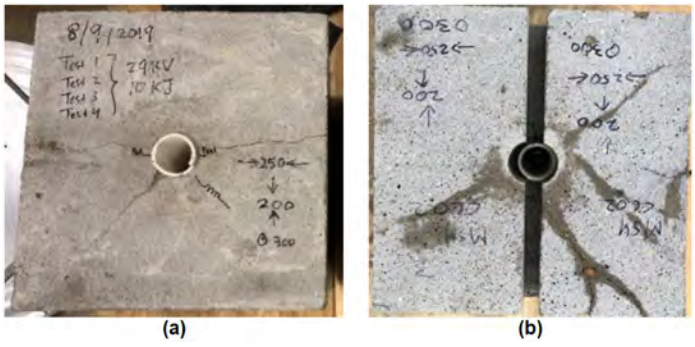

Figure 11—Effect of multiple discharges on the sample with perforation aligned with maximum horizontal stress (a) top of the sample, (b) induced fractures at the slab cut.

Perforations aligned toward maximum horizontal stress direction. It is evident that the fractures tend to propagate toward the maximum compressive stress. In this case, we aligned the PVC pipes perforations toward the direction of maximum horizontal stress, which was 250 psi for this case. Figure 11a-b show the surface of the sample and a slab from the depth where the fusible link was located. We did not observe any

major crack after the first and second discharges. However, after the third discharge, some minor fractures appeared in the samples, and they extended further after the fourth discharge.

Perforations orthogonal toward maximum horizontal stress direction. In the next set of experiments, we aligned the perforations toward the minimum horizontal direction. Like the previous case, we did not observe any visible fractures after the first and second discharges. However, after the third discharge, some visible hair-like fractures formed on the surface of the sample. Finally, after the fourth discharge, more fractures were created on the surface of the sample, and existing fractures extended further. However, the induced cracks in the rock were much less than what we observed in the parallel case. Figure 12 shows the surface (Figure 12a) and in front of the fusible links (Figure 12b) of the used sample for this set of experiments after the fourth discharge. The hair-like fractures in the figures are marked with red arrows in the pictures.

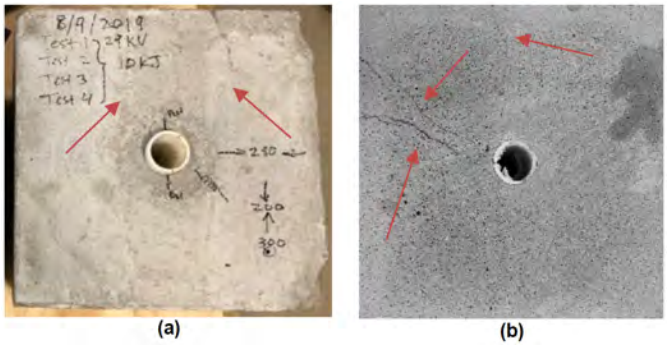

Figure 12—Effect of multiple discharges on the sample with perforation orthogonal to maximum horizontal stress (a) top of the sample, (b) induced fractures at the slab cut.

Comparing Figure 11 and 12, one can conclude the number of fractures is maximized if the perforation direction is aligned to the maximum horizontal stress direction. This observation will be further investigated using metal pipes as casing, elevated stresses, and larger stress anisotropy and the results will be reported in future studies. As a summary of this section, we observed three major and one narrow fracture on the surface of the sample in the parallel case after four discharges, while no major tensile crack was observed on the surface of the fracture in the orthogonal case. Also, we observed that the surface fractures for both parallel and perpendicular cases extended to the middle of the block, where fusible links were located. Finally, we detected that the casing of the parallel sample was destroyed more than the one in the orthogonal case.

Conclusion

In this paper, we investigated the effect of the electrohydraulic pulse generated plasma on the permeability enhancement around a wellbore. We tested discharges ranging from 2 kJ to 12 kJ on nine different rock samples. The samples included three blocks of cement, three sandstones, and three limestones. We also tested four repetitive 10 kJ magnitude shockwaves on two cement samples under confined stresses. Our goal in this study was to stay below the required energy for creating major fractures (destroying the rock completely) in the rock, focusing on the permeability enhancement around the wellbore. The results show that the method can change the permeability of the near-wellbore regions by creating hair-like fractures, even for cases where the output energy is in a range that no major tensile fracture is observed. Also, better enhancement of permeability was observed by multiple discharges. We observed that for the cases with applied confining stresses, much more energy level is required to break the rock. Cement samples showed that the sample under confining stresses did not experience a major tensile fracture (the case of confining stress and multiple fractures), while the sample without confining stresses broke into three pieces after applying 6 kJ discharge. In our future studies, we will present a relationship between the discharge energy

and pressure at the wellbore to have better control of the imposed pressure on the rock sample. Also, since the permeability of the rocks that we tested in this study was relatively high, and the rocks were fairly homogenous, low permeability and heterogeneous rocks will be investigated in the future.

Acknowledgments

The authors of this paper would like to express their sincere appreciation for the financial and technical support they have received from ExxonMobil Corporate Strategic Research. They would also like to express their thanks to ExxonMobil management for approval to publish this manuscript.

References

Ageev, P. G., Ageev, N. P., Pashchenko, A. F., Kasilov, V. P., Ganiev, S. R., & Kurmenev, D. V. (2019). Experimental Study of Plasma-Impulse Impact: Intensity of Pressure Pulsations in the Medium Processed. *Journal of Machinery Manufacture and Reliability*, **48**(2), 184–189.

Bian, D., Zhao, J., Niu, S., & Wu, J. (2018). Rock Fracturing under Pulsed Discharge Homenergic Water Shock Waves with Variable Characteristics and Combination Forms. *Shock and Vibration*, 2018.

Chen, W., C. La Borderie, O. Maurel, G. Pijaudier-Cabot, and F. Rey-Bethbender. (2013). "Simulation of damage–permeability coupling for mortar under dynamic loads." *Int. J. Numer. Anal. Meth. Geomech*. doi:10.1002/nag.2212.

Chen, W., O. Maurel, C. La Borderie, T. Reess, A. De Ferron, M. Matallah, G. Pijaudier-Cabot, A. Jacques, and F. Rey-Bethbender. (2014). "Experimental and numerical study of shock wave propagation in water generated by pulsed arc electrohydraulic discharges." *Heat Mass Transfer* **50**: 673. doi:10.1007/s00231-013-1262-4.

Ghosh, D., and D. A. R. Kay. (1977). "Standard Free Energy of Formation of Alumina." *Journal of The Electrochemical Society* **124** (12): 1836. doi:10.1149/1.2133172.

Grinenko, A., V. Tz. Gurovich, A. Saypin, S. Efimov, and Ya. E. Krasik. (2005). "Strongly coupled copper plasma generated by underwater electrical wire explosion." *Physical Review E* **72** (6): 066401. doi:10.1103/PhysRevE.72.066401.

Grinenko, A., Ya E. Krasik, S. Efimov, A. Fedotov, and V. Tz Gurovich. (2006). "Nanosecond time scale, high power electrical wire explosion in water." *Physics of Plasmas* **13** (4): 042701. doi:10.1063/1.2188085.

Han, Ruoyu, Haibin Zhou, Jiawei Wu, Aici Qiu, and Weidong Ding. (2017). "Relationship between energy deposition and shock wave phenomenon in an underwater electrical wire explosion." *Physics of Plasmas* **24** (9): 093506. doi:10.1063/1.4989790.

Han, Ruoyu, Jiawei Wu, Aici Qiu, Weidong Ding, and Yongmin Zhang. (2018). "Electrical explosions of Al, Ti, Fe, Ni, Cu, Nb, Mo, Ag, Ta, W, W-Re, Pt, and Au wires in water: A comparison study." *Journal of Applied Physics* **124** (4): 043302. doi:10.1063/1.5030760.

Koutoula, Sotiria G., Igor V. Timoshkin, Martin D. Judd, Scott J. MacGregor, and Mark P. Wilson. (2016). "A Study of Energy Partition During Arc Initiation." *IEEE Transactions on Plasma Science* **44** (10): 2137–2144. doi:10.1109/TPS.2016.2579312.

Krasik, Ya E., A. Grinenko, S. Efimov, A. Sayapin, A. Fedotov, V. Tz Gurovich, D. Veksler, J. Felsteiner, and V. Oreshkin. (2007). "Underwater electrical wire explosion." *16th IEEE International Pulsed Power Conference* **2**: 951–956. doi:10.1109/PPPS.2007.4652348.

Krasik, Yakov E., Sergei Efimov, Daniel Sheftman, Alexander Fedotov-Gefen, Oleg Antonov, Daniel Shafer, David Yanuka. (2016). "Underwater Electrical Explosion of Wires and Wire Arrays and Generation of Converging Shock Waves." *IEEE Transactions on Plasma Science* **44** (4): 412–431. doi:10.1109/TPS.2015.2513757.

Kusaiynov, K., N. N. Shuyushbayeva, B. R. Nusupbekov, K. M. Turdybekov, K. M. Shaimerdenova, and B. A. Akhmadiev. (2015). *"Microstructural analysis of the positive electrode of electrohydraulic drill."* **60** (12): 1884–1886. doi:10.1134/S1063784215120105.

Kuznetsova, N. S., A. S. Yudin, and N. V. Voitenko. (2015). "Generation of Shock-Wave Disturbances at Plasma-Vapor Bubble Oscillation." *Journal of Physics: Conference Series* **652** (1): 012037. doi:10.1088/1742-6596/652/1/012037.

Kuznetsova, N. S., V. V. Lopatin, and A. S. Yudin. (2014). "Effect of electro-discharge circuit parameters on the destructive action of plasma channel in solid media." *Journal of Physics: Conference Series* **552** (1): 012029. doi:10.1088/1742-6596/552/1/012029.

La Borderie, C., Reess, T., Chen, W., Maurel, O., Rey-Berbeder, F., & De Ferron, A. (2016). *Electrohydraulic Fracturing of Rocks*. John Wiley & Sons.

Li, Xian Dong, Yi Liu, Si Wei Liu, Zhi Yuan Li, Gu Yue Zhou, Hua Li, Fu Chang Lin, and Yuan Pan. (2016). "Influence of deposited energy on shock wave induced by underwater pulsed current discharge." *Physics of Plasmas* **23** (10): 103104. doi:10.1063/1.4964663.

Liu, Haoyu, Junping Zhao, Geqi Li, and Qiaogen Zhang. (2018). "Spatial and temporal distribution characteristics of an exploding aluminum wire immersed in argon gas." *Physics of Plasmas* **25** (11): 113502. doi:10.1063/1.5055930.

Maurel, O., T. Reess, M. Matallah, A. De Ferron, W. Chen, C. La Borderie, C. Pijauderie, A. Jacques, and F. Rey-Bethbender. (2010). "Electrohydraulic shock wave generation as a means to increase intrinsic permeability of mortar." *Cement and Concrete Research* **40** (12): 1631–1638. doi:10.1016/j.cemconres.2010.07.005.

Melton, N. M., & Cross, T. S. (1968). Fracturing oil shale with electricity. *Journal of Petroleum Technology*, **20**(01), 37–41.

Orlenko, L. P., and L. P. Parshev. (1967). "Calculation of the energy of a shock wave in water." *Journal of Applied Mechanics and Technical Physics* **6** (5): 90–91. doi:10.1007/BF00913396.

Rafiee, M., Rezaei, A., & Soliman, M. (2015). Investigating hydraulic fracture propagation in multi-well pads: a close look at stress shadow from overlapping fractures. *Hydraulic Fracturing Journal*, **2**, 23–27.

Reess, T., De Ferron, A., Maurel, O. (2009). "Electrohydraulic Shock Wave Generation as A Mean to Increase Intrinsic Permeability of Concrete," IEEE Pulsed Power Conference pp.1079–1084, June 29-July 2, Washington DC, USA.

Rezaei, A., Rafiee, M., Soliman, M., & Morse, S. (2015). Investigation of sequential and simultaneous well completion in horizontal wells using a non-planar fully coupled hydraulic fracture simulator. In *49th US Rock Mechanics/ Geomechanics Symposium*. American Rock Mechanics Association.

Riu, H., Jang, H. S., Lee, B. J., Wu, C., & Jang, B. A. (2019). Laboratory-scale fracturing of cement and rock specimen by plasma blasting. *Episodes Journal of International Geoscience*, **42**(3), 213–223.

Rososhek, A., S. Efimov, M. Nitishinski, D. Yanuka, S. V. Tewari, V. Tz Gurovich, K. Khishchenko, and Ya E. Krasik. 2017. "Spherical wire arrays electrical explosion in water and glycerol." *Physics of Plasmas* **24** (12): 122705. doi:10.1063/1.5000037.

Rososhek, A., S. Efimov, S. V. Tewari, D. Yanuka, K. Khishchenko, and Ya E. Krasik. (2018). "Comparison of electrical explosions of spherical wire arrays in water and glycerol on different timescales." *Physics of Plasmas* **25** (6): 062709. doi:10.1063/1.5027145.

Safari, M. R., Gandikota, R., Mutlu, U., Ji, W. M., Glanville, J., & Abass, H. (2013). Pulsed fracturing in shale reservoirs: Geomechanical aspects, ductile-brittle transition and field implications. *In Unconventional resources technology conference* (pp. 448–461). Society of Exploration Geophysicists, American Association of Petroleum Geologists, Society of Petroleum Engineers.

Soliman, M. Y., & Dusterhoft, R. (2016). *Fracturing Horizontal Wells*. McGraw Hill Professional.

Touya, G and Reess, T and Pecastaing, L and Gibert, A and Domens, P. (2006). "Development of subsonic electrical discharges in water and measurements of the associated pressure waves." *Journal of Physics D: Applied Physics* 5236.

Veksler, Dekel, Arkady Sayapin, Sergey Efimov, and Yakov E. Krasik. (2009). "Characterization of Different Wire Configurations in Underwater Electrical Explosion." *IEEE Transactions on Plasma Science* **37** (1): 88–89. doi:10.1109/TPS.2008.2006176.

Voitenko, N. V., A. S. Yudin, and N. S. Kuznetsova. (2015). "Evaluation of Energy Characteristics of High Voltage Equipment for Electro-Blasting Destruction of Rocks and Concrete." *Journal of Physics: Conference Series* **652** (1): 012011. doi:10.1088/1742-6596/652/1/012011.

Xiao, Y., House, W., Unal, E., & Soliman, M. Y. (2018). Pulsed Power Plasma Stimulation Technique–Experimental Study on Single Pulse Test for Fractures Initiation. *SPE Unconventional Resources Technology Conference*, Houston, Texas.

Yanuka, D, A Rososhek, S Theocharous, S N Bland, Ya E Krasik, M P Olbinado, and A Rack. (2018). "Multi-frame synchrotron radiography of pulsed power driven underwater single wire explosions." *Journal of Applied Physics* **124** (15): 153301. doi:10.1063/1.5047204.

Zhao, Junping, Zhuo Xu, Wenyu Yan, Haoyu Liu, and Qiaogen Zhang. (2017). "Characteristics and Diffusion of Electrical Explosion Plasma of Aluminum Wire in Argon Gas." *IEEE Transactions on Plasma Science* **45** (2): 184–192. doi:10.1109/TPS.2017.2651032.

Zhou, Haibin, Ruoyu Han, Qiaojue Liu, Yan Jing, Jiawei Wu, Yongmin Zhang, Aici Qiu, and Youzhi Zhao. (2015a). "Generation of Electrohydraulic Shock Waves by Plasma-Ignited Energetic Materials: II. Influence of Wire Configuration and Stored Energy." *IEEE Transactions on Plasma Science* **43** (12): 4009–4016. doi:10.1109/TPS.2015.2469593.

Zhou, Haibin, Yongmin Zhang, Hengle Li, Ruoyu Han, Yan Jing, Qiaojue Liu, Jiawei Wu, Youzhi Zhao, and Aici Qiu. (2015b). "Generation of Electrohydraulic Shock Waves by Plasma-Ignited Energetic Materials: III. Shock Wave Characteristics With Three Discharge Loads." *IEEE Transactions on Plasma Science* **43** (12): 4017–4023. doi:10.1109/TPS.2015.2477357.

Zhu, Lu, Zheng-Hao He, Zhi-Wen Gao, Fa-Li Tan, Xin-Gui Yue, and Jen-Shih Chang. (2014). "Research on the influence of conductivity to pulsed arc electrohydraulic discharge in water." *Journal of Electrostatics* **72** (1): 53–58. doi:10.1016/j.elstat.2013.11.004.